Perfect coherent transfer in an on-chip reconfigurable nanoelectromechanical network

Tian Tian,[1,2,3] Shaochun Lin,[1,2,3] Liang Zhang,[1,2,3] Peiran Yin,[1,2,3] Pu Huang,[4] Changkui Duan,[1,2,3] Liang Jiang,[5] and Jiangfeng Du[1,2,3,*]

[1]*CAS Key Laboratory of Microscale Magnetic Resonance and Department of Modern Physics, University of Science and Technology of China, Hefei 230026, China*

[2]*Hefei National Laboratory for Physical Sciences at the Microscale, University of Science and Technology of China, Hefei 230026, China*

[3]*Synergetic Innovation Center of Quantum Information and Quantum Physics, University of Science and Technology of China, Hefei 230026, China*

[4]*National Laboratory of Solid State Microstructures and Department of Physics, Nanjing University, Nanjing 210093, China*

[5]*Pritzker School of Molecular Engineering, University of Chicago, Chicago, Illinois 60637, USA*

(Received 17 February 2020; revised manuscript received 20 April 2020; accepted 21 April 2020; published 6 May 2020)

Realizing a controllable network with multiple degrees of interaction is a challenge to physics and engineering. Here, we experimentally report an on-chip reconfigurable network based on nanoelectromechanical resonators with nearest-neighbor (NN) and next-nearest-neighbor (NNN) strong couplings. By applying different parametric voltages on the same on-chip device, we carry out perfect coherent transfer in NN and NNN coupled array networks. Moreover, the low-loss resonators ensure the desired evolution to achieve perfect transfer and the demonstration of the parity-dependent phase relation at transmission cycles. The realization of NNN couplings demonstrates the capability of engineering coherent coupling beyond a simple model of a NN coupled array of doubly clamped resonators. Our reconfigurable nanoelectromechanical network provides a highly tunable physical platform and offers the possibilities of investigating various interesting phenomena, such as topological transport, synchronization of networks, as well as metamaterials.

DOI: 10.1103/PhysRevB.101.174303

I. INTRODUCTION

An oscillator network, made up of multiple individual resonators and couplings between these nodes, has huge potential in investigating collective phenomena, such as exotic states [1], symmetry breaking [2], chimera states [3], an Ising machine [4], and synchronization [5]. Recently, a nanoelectromechanical system was proposed and utilized to explore oscillator networks and the associated phenomena [1,6]. For an ideal network, one of the most important targets is increasing the number of individual nodes. Although there are plenty of unit cells in some reported nanomechanical systems [7–10], any cell of these networks cannot be individually tuned once the fabrication is completed, which unfortunately limits the realization of arbitrarily configurable graphs and further integration.

Another challenge is the tunability of individual couplings in a large oscillator network. For example, there are some studies that investigated the quantum dot or the spin in a mechanical resonator [11–18] and explored the possibility of extending the resonators to a large network [19–21]. However, so far, strong coupling was demonstrated between only two nanomechanical pillars [21]. Since the coupling method between nanomechanical resonators is based on the strain distribution, it is evident that the individual tunability of manipulation will decrease as the number of resonators in networks increases. Therefore, realizing a reconfigurable nanomechanical network with excellent individual tunability is necessary, but it has thus far remained elusive.

Built upon our previous works [22,23], here we successfully extend the parametric coupling from one-dimensional nearest-neighbor (NN) high-quality-factor resonators to next-nearest-neighbor (NNN) ones, and we put forward an on-chip reconfigurable nanoelectromechanical network. By controlling external voltages, we first show that the couplings of NN and NNN resonators can be independently changed, and the strong-coupling regime can be reached. Then we demonstrate perfect coherent transfer in NN as well as NNN coupled networks in the same on-chip device. The state of each resonator can be measured by lock-in amplifiers. The experiment unambiguously shows that the input excitation is perfectly transferred to the target resonator at transmission cycles, which is consistent with the theoretical prediction. Finally, we verify the phase coherence of the perfect coherent transfer in different array networks.

II. PERFECT-TRANSFER SCHEME

The perfect-transfer scheme was first proposed in a spin network with N qubits for transferring a quantum state [24], and it was later generalized to a chain of N coupled harmonic oscillators [25]. In the protocol, the Hamiltonian is

$$H = \sum_{j}^{N-1} C_{j,j+1}[a_j^\dagger a_{j+1} + a_{j+1}^\dagger a_j], \tag{1}$$

*djf@ustc.edu.cn

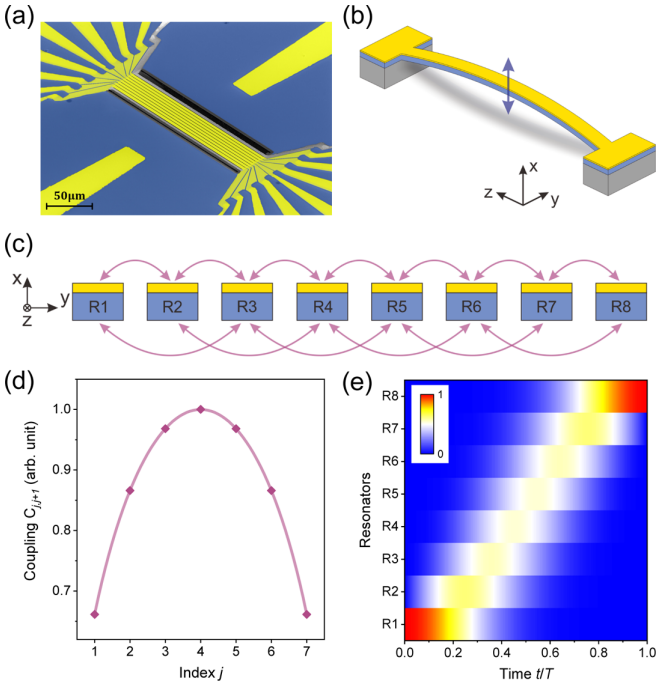

FIG. 1. On-chip reconfigurable nanoelectromechanical network and perfect transfer scheme. (a) False-color scanning electron micrography of the on-chip device, which includes eight nearly identical nanomechanical resonators. The space between adjacent doubly clamped resonators is 500 nm. (b) Sketch map of the geometric structure and the fundamental out-of-plane mode of a 200-μm-long, 3-μm-wide, and 100-nm-thick silicon nitride resonator. These resonators are coated with a 10 nm thin layer of gold to enable electrical manipulation. The magnetic field is applied along the y axis for excitation and detection. (c) The reconfigurable nanoelectromechanical network based on eight resonators with NN and NNN couplings. (d) The couplings of perfect transfer fulfill the relationship $C_{j,j+1} \propto \sqrt{j(N-j)}$ in an array. (e) Perfect coherent transfer from the first site. The color bar stands for excitation amplitudes.

where $a_j^\dagger$ and a_j are the creation and annihilation operators associated with the jth oscillator mode. The coupling $C_{j,j+1}$ describe the interaction between the jth and the $(j+1)$th mode. As shown in Fig. 1(d), when the couplings $C_{j,j+1}$ satisfy the mirror-periodic condition

$$C_{j,j+1} = \frac{C_0}{2}\sqrt{j(N-j)}, \tag{2}$$

a quantum state of the jth qubit can be perfectly transferred to the $(N-j+1)$th qubit after a period $T = \pi/C_0$, where C_0 is the characteristic coupling strength.

To date, the transfer protocol has been demonstrated in nuclear spins [26], optical waveguides [27–29], and superconducting qubits [30]. Actually, the core of this protocol ensures the excited part in the single-excitation subspace, and there is a phase factor $(-1)^{N-1}$ accumulated after a full cycle of forward and backward transfer that only depends on the parity of the number of nodes participating in the transfer protocol [24]. However, the parity-dependent phase relation has not been demonstrated experimentally so far.

III. ON-CHIP RECONFIGURABLE NANOELECTROMECHANICAL NETWORK

In Fig. 1(a), the on-chip nanomechanical system is fabricated by high-stress (1 GPa) silicon nitride, as is detailed in Ref. [22]. Each unit cell of this network is a doubly clamped resonator that is 200 μm long, 3 μm wide, and 100 nm thick. The spacing of NN resonators is about 500 nm. The eight resonators are nearly identical, except for a small difference in the frequencies caused by the variation in length. Actually, we take advantage of this small difference in the first vibration frequencies to realize parametric couplings between adjacent resonators [31]. As shown by the blue arrow in Fig. 1(b), the fundamental mode used is out-of-plane along the x axis for each resonator. To decrease the dissipation and stable frequencies of these nanoelectromechanical resonators, we put this chip in a vacuum chamber of 1.2×10^{-8} mbar and cool it to liquid-nitrogen temperature (77 K). Under this condition, the frequency ranges from 860 to 902 kHz, and quality factors Q reach about 1×10^5. The detailed parameters of eight resonators are listed in the Supplemental Material [32].

In Fig. 1(a) and the cross-section of resonators in Fig. 1(c), the thin layer of gold (golden yellow) on the resonators plays two important roles. First, the layer of gold is an electric conductor for each resonator and it converts the radiofrequency voltages to mechanical oscillation and vice versa, which ensures excitation and measurement in the magnetomotive technique [33]. Second, it provides capacitive interaction with the adjacent resonators and generates excitation hopping between them, assisted by the parametric drive [31].

As shown in Fig. 1(c), all of the nodes (resonators) can be linked by the NN as well as NNN parametric interactions. In this on-chip nanoelectromechanical network, each node can also be controlled and read out by external circuits. We demonstrate this by realizing the linearly tunable couplings and observing perfect coherent transfer in different networks.

A. Nearest-neighbor couplings

As shown in Fig. 2(a), applying voltages V_{dc} together with V_{ac} in one of the NN resonators leads to the coupling between them. Considering the first bias-tee in Fig. 2(a), here the voltage V_{ac} is the sum of $V_{12}\cos(\omega_{12}^{p}t)$ with $\omega_{12}^{p} = \omega_1 - \omega_2$ and $V_{23}\cos(\omega_{23}^{p}t)$ with $\omega_{23}^{p} = \omega_2 - \omega_3$. These voltages V_{12} and V_{23} are used to control the NN parametric couplings C_{12} and C_{23}, respectively.

The experimental result of typical NN parametric coupling is shown in Fig. 2(b), which is measured from the frequency response of the first resonator $R1$. In the measurement, all voltages V_{dc} are chosen as 4 V to keep the frequency difference ω_{12}^{p} unchanged. When $V_{12} = 0$ V, the frequency response suggests the frequency $\omega_1/2\pi = 884.951$ kHz and damping rate $\gamma_1/2\pi = 8.17$ Hz for the first resonator. It is clear that the coupling strength increases linearly with the voltage V_{12} in Fig. 2(b). The coupling reaches about the linewidth when $V_{12} = 0.05$ V and about $18\gamma_1$ when $V_{12} = 0.8$ V [32]. The strong-coupling region ($V_{12} > 0.05$ V) is indicated by the white line in Fig. 2(b). Based on this coupling, we can implement an array network with eight coupled resonators.

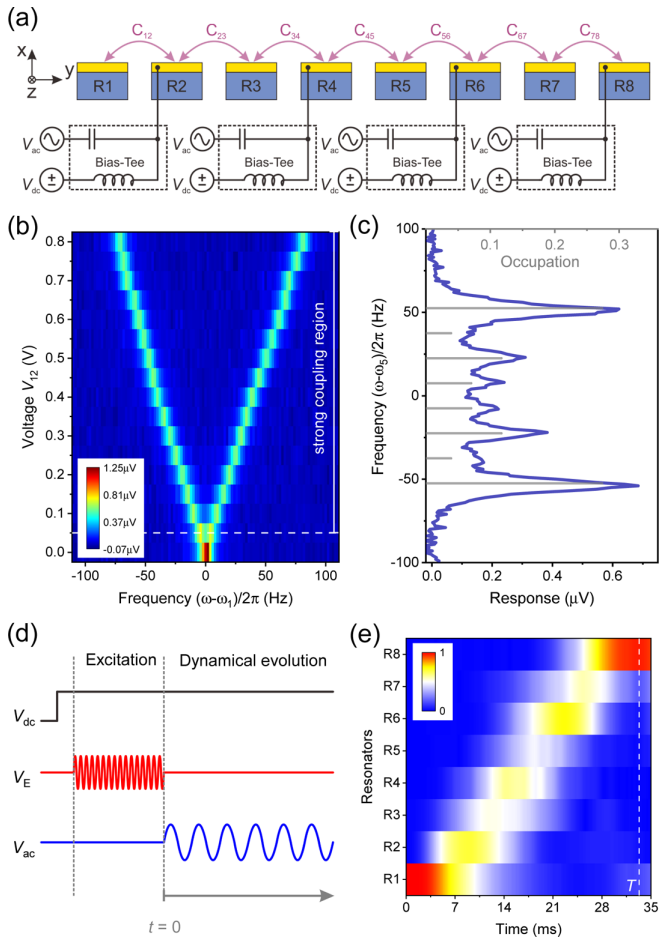

FIG. 2. Perfect coherent transfer in the nearest-neighbor coupled nanomechanical network. (a) Equivalent circuit diagram of controlling NN parametric couplings. The eight resonators are labeled from $R1$ to $R8$ along the y axis. The dc voltage V_{dc} is combined with an ac voltage V_{ac} by a bias tee, where V_{ac} is used to control neighboring couplings $C_{j,j+1}$. The other end of the resonator (along the z axis) is in series with a high resistance (1 MΩ) to make the entire resonator at high potential. (b) Typical parametric coupling between two adjacent resonators under $V_{dc} = 4$ V. It is measured from the first resonator. The coupling strength increases linearly with the ac voltage V_{ac}. (c) The frequency response (dark blue line) at fifth resonator $R5$ under the eight coupled resonators. The gray lines give the theoretical prediction. (d) The pulse sequence in the experiment. (e) The experimental result of the perfect coherent transfer from the first resonator. The color bar denotes normalized amplitudes. The dashed white line marks the moment $T = 33.3$ ms.

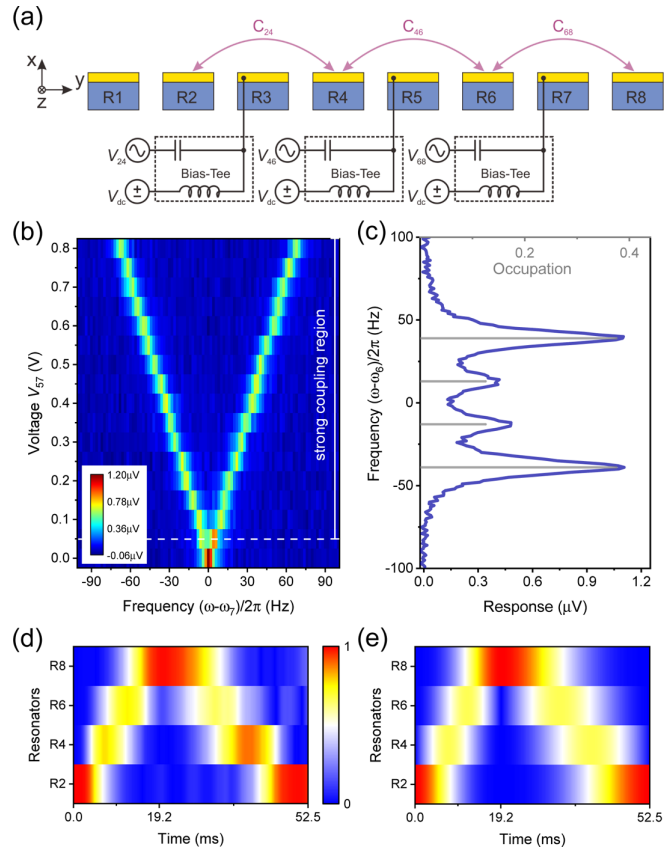

FIG. 3. Perfect coherent transfer in the next-nearest-neighbor coupled nanomechanical network. (a) Equivalent circuit diagram of controlling NNN parametric couplings. The ac voltages V_{24}, V_{46}, and V_{68} are used to control $R2 - R4$, $R4 - R6$, and $R6 - R8$ couplings, respectively. (b) Typical NNN coupling between $R5$ and $R7$ under $V_{dc} = 5.5$ V. The measurement from the seventh resonator. (c) The frequency response (dark blue line) of the sixth resonator $R6$ under the four coupled resonators $R2 - R4 - R6 - R8$ with $C_0 = 2\pi \times 52$ Hz. The gray bars show the theoretical prediction. Experiment (d) and simulation (e) of excitation evolution in the time-dependent network. The first period $T_1 = 19.2$ ms and the second period $T_2 = 33.3$ ms represent coupling $C_0 = 2\pi \times 52$ Hz and $2\pi \times 30$ Hz, respectively.

B. Next-nearest-neighbor couplings

We extend the NN parametric couplings to NNN resonators in the same device. As described in Fig. 3(a), we realize the coupling between the $(j-1)$th and $(j+1)$th resonators by applying voltages in the jth resonator. We show a typical NNN coupling in Fig. 3(b), where V_{dc} and $V_{57}\cos[(\omega_5 - \omega_7)t]$ are combined by a bias-tee and applied to $R6$. Because the capacitance of NNN resonators is smaller than that of NN ones, we set $V_{dc} = 5.5$ V to increase the electrostatic force. This typical NNN coupling is measured at the seventh resonator $R7$. Similar to the NN coupling, the NNN coupling strength also increases linearly with the voltage V_{57}, and it can reach the strong-coupling region when $V_{57} > 0.05$ V. For example, the strength reaches about $18\gamma_7$ when $V_{57} = 0.8$ V. The realization of NNN couplings makes it possible to implement an array network with NNN coupled resonators.

IV. EQUATION OF MOTION

The motion of the jth resonator in the one-dimensional coupled nanoelectromechanical array is described by

$$\ddot{x}_j + \gamma_j \dot{x}_j + \omega_j^2 x_j = P_{j,j+1}(t)(x_{j+1} - x_j) + P_{j-1,j}(t)(x_{j-1} - x_j), \quad (3)$$

where ω_j and γ_j is the eigenfrequency and the damping rate of the jth resonator. $P_{j,j+1}(t) = C_{j,j+1}\cos(\omega^{p}_{j,j+1}t)/m$ is

the dynamic parametric field with coupling strength $C_{j,j+1}$ between the jth and $(j+1)$th resonators. According to the electrostatic force parametric coupling, the coupling $C_{j,j+1}$ is proportional to the product of $V_{\rm dc}$ and $V_{j,j+1}$ [31].

By using the complex amplitude $X_j(t)$ to characterize the dynamics of $x_j = {\rm Re}(X_j e^{i\omega_j t})$ in Eq. (3), we can simplify the dynamical evolution of mechanical oscillation [22]. Under the rotating-wave approximation, $X_j(t)$ obeys the following equation:

$$2i\frac{d}{dt}X_j(t) = C_{j-1,j}X_{j-1}(t) + C_{j,j+1}X_{j+1}(t). \tag{4}$$

Here, the coupling strength $C_{j,j+1}$ is described by angular frequency, and X_j denotes the complex amplitude of the jth resonator. Because all damping of resonators is nearly identical (i.e., $\gamma_1 \approx \gamma_2 \approx \cdots = \gamma$), it only introduces an overall scaling of $\exp[-\gamma t/2]$ of the amplitudes. We can directly compare the normalized amplitudes $X = (X_1, X_2, X_3, \ldots, X_8)^T$ at every moment in experiment with theory. Therefore, we map the dynamical evolution of coupled nanoelectromechanical resonators to a Schrödinger-like equation, which describes the single-excitation tight-binding model in a one-dimensional lattice. For perfect transfer, the period becomes $T = 2\pi/C_0$ because of the factor in Eq. (4).

V. PERFECT COHERENT TRANSFER IN A NEAREST-NEIGHBOR COUPLED NANOMECHANICAL NETWORK

In experiment, by tuning the ac voltage, the NN couplings $C_{j,j+1}$ can satisfy the condition $C_{j,j+1} = C_0\sqrt{j(N-j)}/2$ in Fig. 1(d). Specifically, we choose $C_0 = 2\pi \times 30$ Hz and $N = 8$ in this work. While applying the seven individual NN couplings, we measure the global frequency response at $R5$ to make sure the particular network was realized. As shown in Fig. 2(c), the measured profile of frequency response (dark blue line) is in good agreement with the equidistant theoretical prediction (gray bars), which is crucial for the perfect excitation transfer [25].

Figure 2(d) shows the pulse sequences for measuring excitation transfer. In the whole experimental procedure, all $V_{\rm dc}$ (black line) are high enough to ensure that their frequencies are stable. First, the resonator $R1$ is excited via applying a radiofrequency pulse signal $V_{\rm E}$ (red line). Then, we switch off the excitation source and turn on all $V_{\rm ac}$, which induces excitation transfer across the eight coupled resonators. The measurement is divided into two parts, specifically. The amplitudes of odd resonators are measured when applying voltages into even ones. Similarly, the amplitudes of even resonators can be measured when applying voltages into odd ones [22].

For each part of the dynamical evolution, the amplitudes are demodulated by standard lock-in amplifiers at fixed frequencies of these resonators. To make the results distinct in the whole time domain, we normalize all the amplitudes at each moment; see Fig. 2(e). Obviously, the initial excitation from $R1$ perfectly transfers to $R8$ at the moment $T = 33.3$ ms. Comparing with Fig. 1(e), the experimental result is in agreement with numerical simulation. The minor difference between Figs. 2(e) and 1(e) is caused by ignoring the difference in decay rates of resonators. The original oscillation amplitudes in this process also suggest perfect excitation transfer [32].

VI. PERFECT COHERENT TRANSFER IN A NEXT-NEAREST-NEIGHBOR COUPLED NANOMECHANICAL NETWORK

According to the circuit diagram shown in Fig. 3(a), we apply voltages in $R3$, $R5$, and $R7$ to configure a one-dimensional NNN coupled network $R2 - R4 - R6 - R8$. To meet the condition of Eq. (2) for a chain of four resonators, we set $C_{24} = 2\pi \times 45$ Hz, $C_{46} = 2\pi \times 52$ Hz, and $C_{68} = 2\pi \times 45$ Hz by tuning ac voltages V_{24}, V_{46}, and V_{68}, respectively. This is in accordance with the situation of $C_0 = 2\pi \times 52$ Hz. To confirm the realization of a NNN coupled network, one can check the frequency response of any resonator in the experiment. Figure 3(c) plots the frequency response, which is measured at the sixth resonator $R6$. The dark blue line shows four distinct peaks, in agreement with the equidistant theoretical prediction labeled by gray bars.

We also carry out perfect coherent transfer in the real-time reconfigurable NNN coupled nanomechanical network. More specifically, we configure two structures in the time domain, namely the coupled structure with $C_0 = 2\pi \times 52$ Hz for a one-transmission cycle T_1, and then another structure with $C_0 = 2\pi \times 30$ Hz for T_2. To complete the initial excitation in the edge site, we apply a radiofrequency pulse signal $V_{\rm E}$ at $R2$. After that, all NNN couplings are established by turning on the time-dependent voltages $V_{\rm ac}$. We then measure the dynamical evolution. Lock-in amplifiers demodulate the real-time oscillation amplitudes of $R2$, $R4$, $R6$, and $R8$. As shown in Fig. 3(d), the behavior of excitation evolution meets the perfect-transfer scheme. It is clear that the excitation initially from $R2$ is transferred to $R8$ at time $T_1 = 19.2$ ms and returns to $R2$ at $T_1 + T_2 = 52.5$ ms. The experimental result is in agreement with the numerical simulation [as shown in Fig. 3(e)].

VII. VERIFICATION OF THE PARITY-DEPENDENT PHASE RELATION

In Fig. 4, we experimentally verify the phase coherence associated with the perfect transfer from different initial excitation. After a full cycle of forward and backward transfer, the excitation will reappear at the launching site, with a phase change that depends on the number of oscillators, N. In Figs. 4(a) and 4(b), we measure the dynamical evolution for the input excitation at $R2$ ($R4$) in the NNN coupled network with $N = 4$ resonators. At time T the forward transfer is completed, with excitations transferred to the targeted mirror-symmetric site $R8$ ($R6$). At time $2T$, a full cycle of forward and backward transfer is completed, with all excitations reappearing at the launching site. Moreover, we also measured a π phase shift for an oscillator network with $N = 4$ in Figs. 4(c) and 4(d), regardless of the launching site of the excitation, which is consistent with the theoretical prediction of phase accumulation of $(-1)^{N-1}$ [24].

Figures 4(e) and 4(f) show the perfect coherent transfer for initial excitation at $R1$ and $R3$ in the NN coupled network with $N = 5$ resonators, respectively. At time $2T$, there is

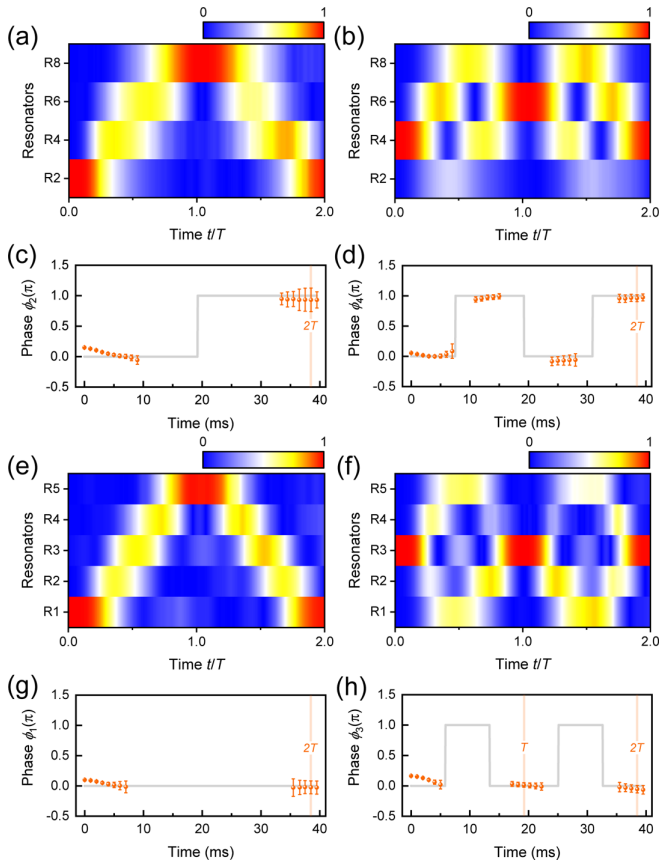

FIG. 4. Dynamics of perfect coherent transfer for the NNN coupled network with $N = 4$ (a)–(d) and the NN coupled network with $N = 5$ (e)–(h). The evolution of amplitude distribution over the relevant oscillator nodes (a,b,e,f) and the phase evolution at the excitation launching site (c,d,g,h), with different choices of launching sites. At time $2T$, we observe a π phase shift for an oscillator network with even $N = 4$ (c,d), while we see no phase shift for odd $N = 5$ (g,h), regardless of the choice of the launching site. Error bars show one standard deviation for 500 repetitions of the experiment. All gray lines are numerical results of quantum mechanics. We choose the same $C_0 = 2\pi \times 52$ Hz for the two networks. The light orange lines stand for the moment $t = T$ and $t = 2T$.

no phase shift when excitations reappeared at the launching site, consistent with the theory prediction of phase change of $(-1)^{N-1}$ that is trivial for odd N. Thanks to the fact that the target resonator is the same as the initially excited one in Fig. 4(f), we can further confirm that the phase variation is zero at time T from Fig. 4(h). Because the initial demodulation of lock-in amplifiers leads to unreliable data, there are deviations at initial milliseconds in Figs. 4(c), 4(d) 4(g), and 4(h). Other than this, the experimental data are consistent with the numerical simulation.

VIII. CONCLUSION

In conclusion, we realize a reconfigurable nanoelectromechanical network and demonstrate perfect coherent transfer in this on-chip device with different array networks. The system exhibits excellent reconfigurability to engineer various energy bands in the same on-chip device, which is crucial to the development of multifunctional and integrative nanomechanical metamaterials [34]. Moreover, the electrically controllable NNN coupling breaks the hamper of spatial dimensions, which makes this platform more feasible to study pattern recognition [35] and explore topology at high dimensions [36–39]. Finally, the coupling method presented in this work shows outstanding tunability in oscillator networks, and this may also be employed in hybrid quantum computing architectures [19].

ACKNOWLEDGMENTS

This work was supported by the National Key R&D Program of China (Grant No. 2018YFA0306600), the Chinese Academy of Sciences (Grants No. GJJSTD20170001 and No. QYZDY-SSW-SLH004), and Anhui Initiative in Quantum Information Technologies (Grant No. AHY050000). P.H. acknowledges support by the National Natural Science Foundation of China (Grant No. 11675163).

T.T. and S.L. contributed equally to this work.

[1] M. H. Matheny, J. Emenheiser, W. Fon, A. Chapman, A. Salova, M. Rohden, J. Li, M. Hudoba de Badyn, M. Pósfai, L. Duenas-Osorio *et al.*, Exotic states in a simple network of nanoelectromechanical oscillators, Science **363**, eaav7932 (2019).

[2] F. Molnar, T. Nishikawa, and A. E. Motter, Network experiment demonstrates converse symmetry breaking, Nat. Phys. **16**, 351 (2020).

[3] J. D. Hart, K. Bansal, T. E. Murphy, and R. Roy, Experimental observation of chimera and cluster states in a minimal globally coupled network, Chaos **26**, 094801 (2016).

[4] A. Marandi, Z. Wang, K. Takata, R. L. Byer, and Y. Yamamoto, Network of time-multiplexed optical parametric oscillators as a coherent Ising machine, Nat. Photon. **8**, 937 (2014).

[5] C. A. Holmes, C. P. Meaney, and G. J. Milburn, Synchronization of many nanomechanical resonators coupled via a common cavity field, Phys. Rev. E **85**, 066203 (2012).

[6] W. Fon, M. H. Matheny, J. Li, L. Krayzman, M. C. Cross, R. M. D'Souza, J. P. Crutchfield, and M. L. Roukes, Complex dynamical networks constructed with fully controllable nonlinear nanomechanical oscillators, Nano Lett. **17**, 5977 (2017).

[7] A. A. Awad, P. Dürrenfeld, A. Houshang, M. Dvornik, E. Iacocca, R. K. Dumas, and J. Åkerman, Long-range mutual synchronization of spin Hall nano-oscillators, Nat. Phys. **13**, 292 (2017).

[8] J. Cha, K. W. Kim, and C. Daraio, Experimental realization of on-chip topological nanoelectromechanical metamaterials, Nature (London) **564**, 229 (2018).

[9] J. Cha and C. Daraio, Electrical tuning of elastic wave propagation in nanomechanical lattices at MHz frequencies, Nat. Nanotech. **13**, 1016 (2018).

[10] D. Hatanaka, I. Mahboob, K. Onomitsu, and H. Yamaguchi, Phonon waveguides for electromechanical circuits, Nat. Nanotech. **9**, 520 (2014).

[11] S. D. Bennett, N. Y. Yao, J. Otterbach, P. Zoller, P. Rabl, and M. D. Lukin, Phonon-Induced Spin-Spin Interactions in Diamond Nanostructures: Application to Spin Squeezing, Phys. Rev. Lett. **110**, 156402 (2013).

[12] I. Yeo, P.-L. de Assis, A. Gloppe, E. Dupont-Ferrier, P. Verlot, N. S. Malik, E. Dupuy, J. Claudon, J.-M. Gérard, A. Auffèves *et al.*, Strain-mediated coupling in a quantum dot-mechanical oscillator hybrid system, Nat. Nanotech. **9**, 106 (2014).

[13] M. Montinaro, G. Wüst, M. Munsch, Y. Fontana, E. Russo-Averchi, M. Heiss, A. Fontcuberta i Morral, R. J. Warburton, and M. Poggio, Quantum dot opto-mechanics in a fully self-assembled nanowire, Nano Lett. **14**, 4454 (2014).

[14] P. Ovartchaiyapong, K. W. Lee, B. A. Myers, and A. C. Bleszynski Jayich, Dynamic strain-mediated coupling of a single diamond spin to a mechanical resonator, Nat. Commun. **5**, 4429 (2014).

[15] J. Teissier, A. Barfuss, P. Appel, E. Neu, and P. Maletinsky, Strain Coupling of a Nitrogen-Vacancy Center Spin to a Diamond Mechanical Oscillator, Phys. Rev. Lett. **113**, 020503 (2014).

[16] K. W. Lee, D. Lee, P. Ovartchaiyapong, J. Minguzzi, J. R. Maze, and A. C. Bleszynski Jayich, Strain Coupling of a Mechanical Resonator to a Single Quantum Emitter in Diamond, Phys. Rev. Appl. **6**, 034005 (2016).

[17] M. Munsch, A. V. Kuhlmann, D. Cadeddu, J.-M. Gérard, J. Claudon, M. Poggio, and R. J. Warburton, Resonant driving of a single photon emitter embedded in a mechanical oscillator, Nat. Commun. **8**, 76 (2017).

[18] S. G. Carter, A. S. Bracker, G. W. Bryant, M. Kim, C. S. Kim, M. K. Zalalutdinov, M. K. Yakes, C. Czarnocki, J. Casara, M. Scheibner *et al.*, Spin-Mechanical Coupling of an InAs Quantum Dot Embedded in a Mechanical Resonator, Phys. Rev. Lett. **121**, 246801 (2018).

[19] P. Rabl, S. J. Kolkowitz, F. H. L. Koppens, J. G. E. Harris, P. Zoller, and M. D. Lukin, A quantum spin transducer based on nanoelectromechanical resonator arrays, Nat. Phys. **6**, 602 (2010).

[20] B. Machielse, S. Bogdanovic, S. Meesala, S. Gauthier, M. J. Burek, G. Joe, M. Chalupnik, Y. I. Sohn, J. Holzgrafe, R. E. Evans *et al.*, Quantum Interference of Electromechanically Stabilized Emitters in Nanophotonic Devices, Phys. Rev. X **9**, 031022 (2019).

[21] J. Doster, S. Hoenl, H. Lorenz, P. Paulitschke, and E. M. Weig, Collective dynamics of strain-coupled nanomechanical pillar resonators, Nat. Commun. **10**, 5246 (2019).

[22] T. Tian, Y. Ke, L. Zhang, S. Lin, Z. Shi, P. Huang, C. Lee, and J. Du, Observation of dynamical phase transitions in a topological nanomechanical system, Phys. Rev. B **100**, 024310 (2019).

[23] L. Zhang, T. Tian, P. Huang, S. Lin, and J. Du, Coherent transfer of excitation in a nanomechanical artificial lattice, Chin. Phys. Lett. **37**, 014501 (2020).

[24] M. Christandl, N. Datta, A. Ekert, and A. J. Landahl, Perfect State Transfer in Quantum Spin Networks, Phys. Rev. Lett. **92**, 187902 (2004).

[25] N. Y. Yao, Z.-X. Gong, C. R. Laumann, S. D. Bennett, L.-M. Duan, M. D. Lukin, L. Jiang, and A. V. Gorshkov, Quantum logic between remote quantum registers, Phys. Rev. A **87**, 022306 (2013).

[26] J. Zhang, G. L. Long, W. Zhang, Z. Deng, W. Liu, and Z. Lu, Simulation of Heisenberg XY interactions and realization of a perfect state transfer in spin chains using liquid nuclear magnetic resonance, Phys. Rev. A **72**, 012331 (2005).

[27] M. Bellec, G. M. Nikolopoulos, and S. Tzortzakis, Faithful communication Hamiltonian in photonic lattices, Opt. Lett. **37**, 4504 (2012).

[28] A. Perez-Leija, R. Keil, A. Kay, H. Moya-Cessa, S. Nolte, L.-C. Kwek, B. M. Rodríguez-Lara, A. Szameit, and D. N. Christodoulides, Coherent quantum transport in photonic lattices, Phys. Rev. A **87**, 012309 (2013).

[29] R. J. Chapman, M. Santandrea, Z. Huang, G. Corrielli, A. Crespi, M.-H. Yung, R. Osellame, and A. Peruzzo, Experimental perfect state transfer of an entangled photonic qubit, Nat. Commun. **7**, 11339 (2016).

[30] X. Li, Y. Ma, J. Han, T. Chen, Y. Xu, W. Cai, H. Wang, Y. P. Song, Z.-Y. Xue, Z.-q. Yin, and L. Sun, Perfect Quantum State Transfer in a Superconducting Qubit Chain with Parametrically Tunable Couplings, Phys. Rev. Appl. **10**, 054009 (2018).

[31] P. Huang, P. Wang, J. Zhou, Z. Wang, C. Ju, Z. Wang, Y. Shen, C. Duan, and J. Du, Demonstration of Motion Transduction based on Parametrically Coupled Mechanical Resonators, Phys. Rev. Lett. **110**, 227202 (2013).

[32] See Supplemental Material at http://link.aps.org/supplemental/10.1103/PhysRevB.101.174303 for an additional detailed description of the theoretical model, the properties of the system, and some numerical results.

[33] A. N. Cleland and M. L. Roukes, External control of dissipation in a nanometer-scale radiofrequency mechanical resonator, Sens. Actuators A **72**, 256 (1999).

[34] N. I. Zheludev and E. Plum, Reconfigurable nanomechanical photonic metamaterials, Nat. Nanotech. **11**, 16 (2016).

[35] D. Vodenicarevic, N. Locatelli, F. Abreu Araujo, J. Grollier, and D. Querlioz, A nanotechnology-ready computing scheme based on a weakly coupled oscillator network, Sci. Rep. **7**, 44772 (2017).

[36] L. Li, Z. Xu, and S. Chen, Topological phases of generalized Su-Schrieffer-Heeger models, Phys. Rev. B **89**, 085111 (2014).

[37] M. Maffei, A. Dauphin, F. Cardano, M. Lewenstein, and P. Massignan, Topological characterization of chiral models through their long time dynamics, New J. Phys. **20**, 013023 (2018).

[38] F. A. An, E. J. Meier, and B. Gadway, Engineering a Flux-Dependent Mobility Edge in Disordered Zigzag Chains, Phys. Rev. X **8**, 031045 (2018).

[39] B. Pérez-González, M. Bello, Á. Gómez-León, and G. Platero, Interplay between long-range hopping and disorder in topological systems, Phys. Rev. B **99**, 035146 (2019).